ChemComm
Chemical Communications

Accepted Manuscript

This article can be cited before page numbers have been issued, to do this please use: S. Su, Q. Sun, J. Ma, D. Zhu, F. Wang, J. Chao, C. Fan, Q. Li and L. Wang, *Chem. Commun.*, 2020, DOI: 10.1039/D0CC03845H.

ROYAL SOCIETY OF CHEMISTRY

rsc.li/chemcomm

View Article Online
DOI: 10.1039/D0CC03845H

ARTICLE

Ultrasensitive analysis of microRNAs with gold nanoparticles-decorated molybdenum disulfide nanohybrids-based multilayer nanoprobes

Received 00th January 20xx,
Accepted 00th January 20xx

DOI: 10.1039/x0xx00000x

Shao Su,[‡a] Qian Sun,[‡a] Jianfeng Ma,[a] Dan Zhu,[a] Fei Wang,[b] Jie Chao,[a] Chunhai Fan,[b] Qian Li*[b] and Lianhui Wang*[a]

Nanoprobes-based signal amplification strategy is a powerful way to ultrasensitively detect biomolecules. Herein, a gold nanoparticles-decorated molybdenum disulfide (MoS_2-AuNPs)-based multilayer nanoprobe (MLNPs) was designed for ultrasensitive analysis of microRNA (miRNA-21). The MLNPs-amplified electrochemical biosensor exhibited ultrawide dynamic range (10 aM-1 μM) and ultralow detection limit (38 aM) for target miRNA-21 analysis. Furthermore, this biosensor can determine miRNA-21 expression in cells lysate of 100 human cervical cancer (HeLa) cells. Our results demonstrate that MoS_2-AuNPs nanocomposites have great potential in constructing biosensors for target molecules analysis.

MicroRNA (miRNA) is an important biomarker related to human diseases occurrence, diagnosis and treatment.[1] To analyze the low expression level of miRNA quantitatively and accurately, it is highly desirable to develop sensitive detection methods.[2,3] Due to their ultrahigh detection sensitivity, methods employing various amplification strategies have attracted extensive research interests, such as real-time quantitative PCR amplification,[4,5] hybridization chain reaction amplification (HCR),[6,7] rolling circle amplification,[8,9] enzyme-assisted amplification[10,11] and nanoprobe-based amplification.[12,13] Besides those, other amplification methods were also designed to sensitively and selectively analyze microRNA.[14-17]

With the great advances of nanotechnology, nanoprobe-based amplification has become a powerful tool to amplify detection signals according to the advantages of nanomaterials, such as large surface area, high chemical stability, easy functionalization and high conductivity.[18] In the research filed of electrochemical sensors/biosensors, nanoprobes have been widely utilized to efficiently improve analysis performance since large amounts of molecular recognition groups, signal reporters and amplifiers can be loaded on them.[19] Up to date, various nanomaterials have been employed to construct nanoprobes,[20] such as noble metal nanostructures,[21] carbon nanotubes,[22] silicon nanowires,[23] metal oxides,[24] graphene and its derivatives.[25] For example, gold nanoparticles (AuNPs)-based nanoprobes have been constructed for target DNA detection by using chronocoulometry (CC) method. Hundreds of DNA strands assembled on a single AuNP to form a nanoprobe, which can greatly amplify electrochemical signals by electrostatic adsorption of $[Ru(NH_3)_6]^{3+}$.[26] By loading two electrochemical indicators (toluidine blue and Prussian blue) and two antibodies (anti-CEA and anti-AFP) on the surface of carboxyl graphene nanosheets (CGS), CEA and AFP can be simultaneously determined.[27]

Due to their unique chemical/physical properties, two-dimensional (2D) layered nanomaterials have been extensively employed to develop nanoprobes for electrochemical signal amplification,[28] including graphene and its derivatives,[29] transition metal chalcogenides (such as MoS_2 and WS_2)[30] and metal oxides (MnO_2).[31] Notably, most of 2D nanomaterials-based probes are single-layer nanostructures. Therefore, the amplification effect of multilayer 2D nanomaterials-based nanoprobes need further exploration. Here, we designed a MoS_2-AuNPs-based multilayer nanoprobe for ultrasensitive analysis of microRNAs. Two nanoprobes (probe 1 and probe 2) were prepared by assembling two thiolated ssDNA (termed as DNA1 and DNA2), which were complementary to each other, respectively (Scheme 1). Thus fabricated probe 1 and probe 2 can easily hybridize with each other to form multilayer nanostructures. Then, another thiol-labelled ssDNA (DNA3) was co-immobilized on the surface of multilayer nanostructures to form MLNPs, which was used to hybridize with target miRNA-21. Consequently, a classical DNA "sandwich" structure was obtained between MCH/DNA4/Au and MLNPs in the presence of miRNA-21. Notably, the impedance value of the MLNPs-constructed electrochemical sensor was larger than that of SLNPs-constructed sensor, which was ascribed to the block of electron transfer by the multilayer nanostructures of MLNPs. Moreover, larger amounts of DNA on MLNPs surface with negative

[a] Key Laboratory for Organic Electronics and Information Displays (KLOEID) & Jiangsu Key Laboratory for Biosensors, Institute of Advanced Materials (IAM), National Synergetic Innovation Center for Advanced Materials (SICAM), Nanjing University of Posts and Telecommunications, 9 Wenyuan Road, Nanjing 210023, China. E-mail: iamlhwang@njupt.edu.cn
[b] School of Chemistry and Chemical Engineering, Shanghai Jiao Tong University, Shanghai 200240, China. E-mail: liqian2018@sjtu.edu.cn
Electronic Supplementary Information (ESI) available: Experimental details and supporting figures. See DOI: 10.1039/x0xx00000x
‡These authors contributed equally.

charge could pull electrochemical indicator $[Fe(CN)_6]^{3-/4-}$ further away from electrode surface due to electrostatic repulsive force.

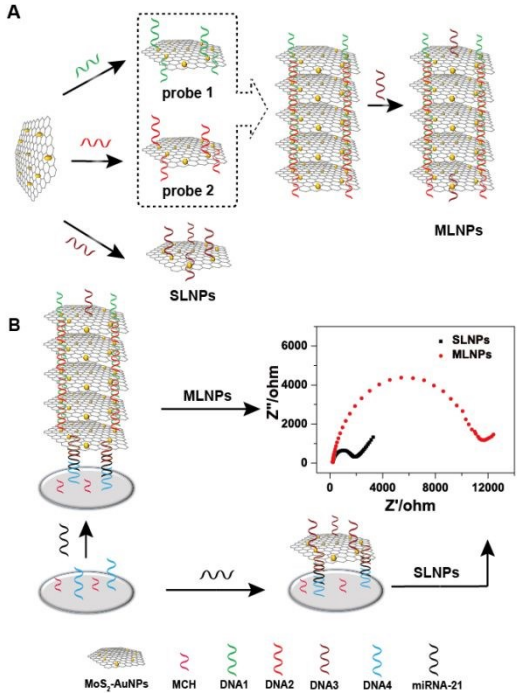

Scheme 1. Schematic illustration of the electrochemical biosensor constructed with MoS_2-AuNPs-based single-layer and multilayer nanoprobes (SLNPs and MLNPs) for ultrasensitive microRNA detection. (A) Scheme of construction of probe 1, probe 2, SLNPs and MLNPs. (B) Scheme of the electrochemical biosensors for microRNA detection constructed with SLNPs and MLNPs.

The zeta potential and dynamic light scattering (DLS) analyses were used to verify the synthesis of SLNPs and MLNPs (Fig. S1, ESI†). The zeta potential of MoS_2-AuNPs, SLNPs, and MLNPs were -16.5±1.5 mV, -20.8±1.0 mV, and -35.5±2.5 mV, respectively. Since the negatively charged DNA assembled on MoS_2-AuNPs surface could result in the negative potential shift, the negative zeta potentials suggested the successful preparation of MoS_2-AuNPs-based nanoprobes. The average diameter of MoS_2-AuNPs nanocomposites were 317.4±12.3 nm. After the formation of nanoprobes, the average diameter increased to 363.9±15.6 nm (SLNPs) and 1231.7±94.2 nm (MLNPs), respectively, also implying the formation of SLNPs and MLNPs. Moreover, the diameter of MLNPs decreased to 564.6±20.4 nm after the thermal denaturation, indicating that MLNPs decomposed to smaller composites due to the dissociation of DNA double strands,[32] which further indicated the success of MLNPs formation.

Atomic force microscope (AFM) was employed to further characterize MLNPs (Fig. S2, ESI†). After decoration of AuNPs, the height of MoS_2-AuNPs nanocomposites was 19.6±1.3 nm (Fig. S2B), which was higher than that of MoS_2 nanosheets (1.8±0.4 nm, Fig. S2A). The increased height (17.8±0.9 nm) is in agreement with the diameter of AuNPs analyzed by TEM image (Fig. S3, ESI†), suggesting AuNPs decorated on MoS_2 surface. The height of MLNPs was in the range of 20-100 nm, indicating that MLNPs was formed with 1-5 layers of MoS_2-AuNPs nanocomposites (Fig. S2C). It was noted that more than 93% MLNPs was composed of two or more layers of MoS_2-AuNPs and the five-layer nanocomposites is the dominate one with a percentage of 62% (Fig. S2D).

The feasibility of these MoS_2-AuNPs-based nanoprobes for electrochemical analysis of miRNA-21 was evaluated by electrochemical impedance spectroscopy (EIS). Typically, the semicircle diameter of EIS was used to reflect the electron transfer resistance. As shown in Figure S4 (ESI†), the impedance of DNA4/Au (1107.2 Ω, curve b) and MCH/DNA4/Au (1385.5 Ω, curve c) was larger than that of the bare Au electrode (328.8 Ω, curve a), which was ascribed to the immobilized DNA4 hindered the electron transfer due to the electrostatic repulsion between DNA and $[Fe(CN)_6]^{3-/4-}$ and 6-mercaptohexanol (MCH) efficiently blocked the remaining active sites. In the presence of miRNA-21, the impedance of miRNA-21/MCH/DNA4/Au increased to 2022.0 Ω (curve e), suggesting miRNA-21 was captured by DNA4/Au. After the addition of SLNPs, the impedance of this biosensor can further increase to 3045.5 Ω (curve f), indicating SLNPs successfully assembled on electrode surface. The impedance reached 11491.1 Ω (curve g) with addition of MLNPs, which was almost 4-fold of the impedance of SLNPs. To figure out the effect of unspecific adsorption of MLNPs on electrode surface, a control experiment was carried out by adding MLNPs in the absence of miRNA-21. The low impedance value (1626.1 Ω, curve d) suggested the existence of weak nonspecific adsorption of MLNPs. Notably, the background signal originated from nonspecific adsorption would not significantly affect detection performance due to the excellent signal amplification effect of MLNPs.

To investigate the signal amplification effect of MLNPs and SLNPs, we employed a layer-by-layer (LBL) method as a control group to compare the electrochemical signals (Fig. 1A). The EIS curves of different MoS_2-AuNPs-based nanoprobes were exhibited in Fig. 1B. Taking the impedance of MCH/DNA4/Au as the blank control, its impedance change ($\Delta R_{ct}=R_{ct,\ signal}-R_{ct,\ blank}$) was about 679.3 Ω in the presence of 100 pM miRNA-21 (Fig. 1C), while the observed ΔR_{ct} was dependent on miRNA-21 concentration. The ΔR_{ct} of electrochemical biosensor amplified by SLNPs was 1831.1 Ω, compared to the one of MLNPs 10103.4 Ω, suggesting a superior signal amplification effect of MLNPs. In the case of LBL assembly, the impedance increased continuously with the layers increased from 1 to 3, while suddenly dropped for the 4-layer assembly (Fig. S5, ESI†). It may be ascribed to the assemble limit of LBL nanoprobes on electrode surface. Another possible reason was that some LBL nanoprobes fell off electrode surface during the repeated incubation and cleaning process. The ΔR_{ct} of 3-layer LBL was 4826.4 Ω, which was 2.6 folds of SLNPs and 0.48 folds of MLNPs, further suggesting a superior signal amplification effect of one-step MLNPs to SLNPs and multi-steps LBL process. Meanwhile, the fold changes of electrochemical signal assembled with MLNPs, LBL nanoprobe, SLNPs and only miRNA compared with blank control also supported this conclusion (Fig. 1C).

View Article Online
DOI: 10.1039/D0CC03845H

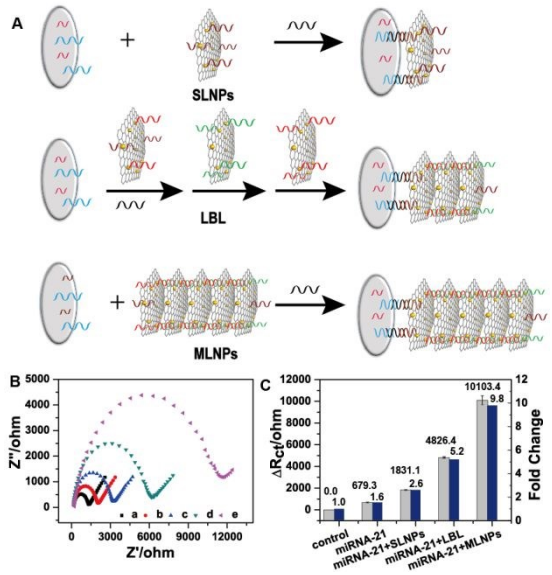

Fig. 1 Signal amplification effect of MLNPs and SLNPs. (A) Schematic illustration of electrochemical biosensors constructed by SLNPs, LBL nanoprobe and MLNPs. (B) EIS curves of (a) MCH/DNA4/Au, (b) miRNA-21/MCH/DNA4/Au, (c) SLNPs/miRNA-21/MCH/DNA4/Au, (d) 3-layer LBL probes/miRNA-21/MCH/DNA4/Au and (e) MLNPs/miRNA-21/MCH/DNA4/Au. (C) The values of corresponding impedance change were obtained by three MoS_2-based nanoprobes.

We investigated the miRNA-21 detection performance of the MLNPs-amplified electrochemical sensor, taking SLNPs-amplified sensor as the control. In order to eliminate the influence of different electrodes, we defined $\Delta R_{ct}/R_{ct}$ ($(R_{ct,\ miRNA}-R_{ct,\ no\ miRNA})/R_{ct,\ no\ miRNA}$) to evaluate the detection performance of these two biosensors, in which $R_{ct,\ no\ miRNA}$ was the impedance value of MCH/DNA4/Au, and $R_{ct,\ miRNA}$ was the impedance value of SLNPs or MLNPs when assembled on the surface of MCH/DNA4/Au in the presence of miRNA-21. Figure 2A showed that the $\Delta R_{ct}/R_{ct}$ values of the SLNPs-amplified electrochemical biosensor, which increased in the presence of 1 fM-1 nM miRNA-21 and reached a plateau at the miRNA-21 concentration of 1 nM (Fig. S6A, ESI†). A linear relationship was obtained between the $\Delta R_{ct}/R_{ct}$ value and the logarithm value of miRNA-21 concentration in the range of 1 fM-1 nM with a detection limit of 0.29 fM (Fig. 2B). In the case of MLNPs-amplified electrochemical biosensor (Fig. S6B, ESI†), an ultrawide dynamic range (0.01 fM-1 μM) was observed (Fig. 2A). Two linear ranges for the miRNA-21 concentration of 0.1 fM-10 pM and 10 pM-1 μM with a corresponding linear equation y=0.17x-0.17 (R^2=0.98) and y=0.41x-1.82 (R^2=0.99), respectively. The detection limit of the MLNPs-based biosensor was calculated to be 0.038 fM (S/N=3), which was almost an order of magnitude lower than that of the SLNPs-based biosensor (0.29 fM). Furthermore, the analytical performance of MLNPs-amplified electrochemical biosensor included linear range and detection limit was compared to other published works (Fig. 2C), suggesting the MLNPs-amplified electrochemical biosensor show better analytical performance with a wider dynamic range and lower detection limit for miRNA-21 detection. We also compared the detection selectivity of SLNPs-amplified and MLNPs-amplified electrochemical biosensors (Fig. S7, ESI†). For single-base mismatch miRNA (SM-miRNA) and miRNA-486, the $\Delta R_{ct}/R_{ct}$ of SNLPs-amplified electrochemical biosensor was 0.47 and 0.24 folds of the one for miRNA-21, respectively. Whereas $\Delta R_{ct}/R_{ct}$ of MLNPs-amplified biosensors was 0.30 and 0.17 folds of the one for miRNA-21, respectively (Fig. 2D). Therefore, the MLNPs-amplified electrochemical biosensor showed better selectivity for target miRNA-21 analysis.

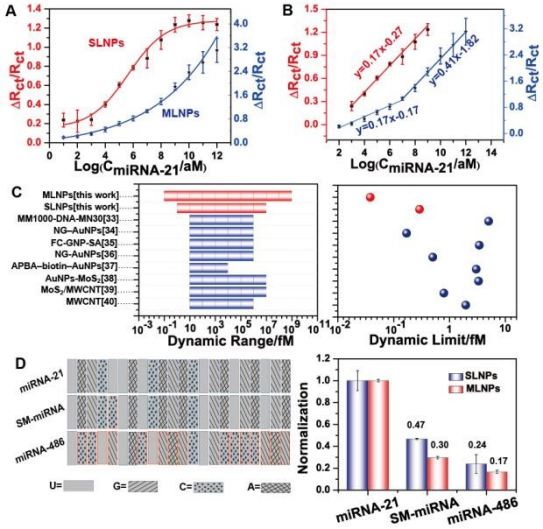

Fig. 2 Analytical performance of SLNPs-amplified and MLNPs-amplified electrochemical sensors. (A) The dynamic ranges and (B) the corresponding calibration curves of SLNPs-amplified and MLNPs-amplified electrochemical biosensors for 10 aM-1 μM miRNA-21 detection. (C) The comparison of analytical performance of our biosensors and other published works. (D) Selectivity of SLNPs-amplified and MLNPs-amplified electrochemical biosensors for the detection of miRNA-21, SM-miRNA and miRNA-486, respectively. The concentrations of all miRNAs were 100 pM.

To evaluate the practicability of this MLNPs-amplified electrochemical biosensor, we simulated a real detection strategy by adding miRNA-21 into human serum (Fig. 3A). The recovery of this biosensor was over 95% and the relative standard deviation (RSD) was below 6%, suggesting the MLNPs-amplified electrochemical biosensor possessed an acceptable detection performance (Table S1, ESI†). Furthermore, human cervical cancer (HeLa) cells with high miRNA-21 expression and normal liver cancer (L-O2) cells with low miRNA-21 expression were selected to evaluate the practical application of MLNPs-amplified electrochemical biosensor in cellular miRNA detection. The impedance of the MNLP-amplified electrochemical biosensor increased with the number of HeLa cells ranging from 10-10^6 (Fig. S8, ESI†), while as a control, the impedance of this biosensor showed no difference when detecting 10-10^6 L-O2 cells. Notably, the MLNPs-amplified electrochemical biosensor can efficiently determine the expression of miRNA-21 in 10 and 100 HeLa cells ($P<0.05$, Fig. 3B). Taken together, our proposed biosensor had great potential for detecting miRNAs in real samples and tumor cells.

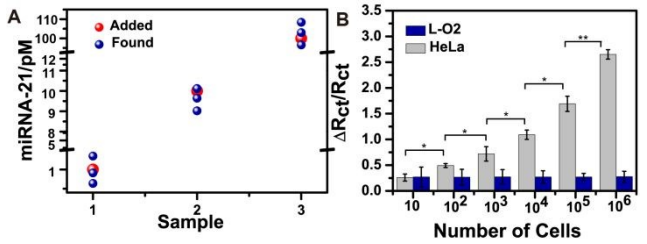

Fig. 3 Analysis of miRNA-21 in (A) human serum and (B) lysates of HeLa cells and L-O2 cells by using the MLNPs-amplified electrochemical biosensor. Statistical significance of miRNA-21 expression in HeLa cells analyzed by Student t-test; *P<0.05 and **P<0.01. Error bars show standard deviations from three independent experiments.

In this work, we successfully developed a high-performance electrochemical biosensor for miRNA-21 detection by using MoS_2-based multilayer nanoprobes as signal amplifiers, which exhibited an ultrawide dynamic range and an ultralow detection limit. Moreover, the MLNPs-amplified biosensor showed excellent selectivity for the discrimination of single-base mismatch miRNAs, which could determine miRNA-21 expression in cell lysates of 100 HeLa cells. MoS_2-AuNPs-based multilayer nanoprobes can integrated different single-layer MoS_2-based nanoprobes with functionalized groups, which can give the multilayer nanoprobes more functionalization and better analysis performance. Therefore, MLNPs were promising signal-amplified nanoprobes to construct biosensors for in vitro and in vivo target molecules analysis combined with different detection techniques.

This work was supported by the National Key Research and Development Program of China (2017YFA0205302), the National Natural Science Foundation of China (61671250 and 21475064), the Key Research and Development Program of Jiangsu (BE2018732), the Natural Science Key Fund for Colleges, Universities in Jiangsu Province (17KJA430011), the Priority Academic Program Development of Jiangsu Higher Education Institutions (PAPD, YX030003) and the Scientific Research Foundation of Nanjing University of Posts and Telecommunications (NY218032).

Conflicts of interest

There are no conflicts of interest to declare.

Notes and references

1 L. Zhang, S. Zhang, J. Yao, F. J. Lowery, Q. Zhang, W. C. Huang, P. Li, M. Li, X. Wang and C. Zhang, *Nature*, 2015, **527**, 100-104.
2 M. Labib, N. Khan, S. M. Ghobadloo, J. Cheng, J. P. Pezacki and M. V. Berezovski, *J. Am. Chem. Soc.*, 2013, **135**, 3027-3038.
3 K. Y. Zhang, S. T. Song, S. Huang, L. Yang, Q. H. Ma, X. C. Wang, F. Lin and J. J. Zhang, *Small*, 2018, **14**, 1802292.
4 H. J. Lee, B. C. Kim, K. W. Kim, Y. K. Kim, J. Kim and M. K. Oh, *Biosens. Bioelectron.*, 2009, **24**, 3550-3555.
5 K. Lao, N. L. Xu, V. Yeung, C. Chen, K. J. Livak and N. A. Straus, *Biochem. Bioph. Res. Co.*, 2006, **343**, 85-89.
6 J. Chao, Z. Li, J. Li, H. Peng, S. Su, Q. Li and L. H. Wang, *Biosens. Bioelectron.*, 2016, **81**, 92-96.
7 H. Chu, J. Zhao, Y. Mi, Y. Zhao and L. Li, *Angew. Chem. Int. Ed.*, 2019, **58**, 14877.
8 Y. Zhu, H. Wang, L. Wang, J. Zhu and W. Jiang, *ACS Appl. Mater. Interface*, 2016, **8**, 2573-2581.
9 B. Tian, Z. Qiu, J. Ma, M. Donolato, M. F. Hansen, P. Svedlindh and M. Strömberg, *ACS Appl. Mater. Interface,* 2018, **10**, 2957-2964.
10 S. Bi, J. Zhang and S. Zhang, *Chem. Commun.*, 2010, **46**, 5509-5511.
11 W. Zhao, M. Liu, H. Li, S. Wang, S. Tang, R. M. Kong and R. Yu, *Biosens. Bioelectron.*, 2019, **143**, 111593.
12 X. Miao, Z. Cheng, H. Ma, Z. Li, N. Xue and P. Wang, *Anal. Chem.*, 2017, **90**, 1098-1103.
13 S. Su, Q. Sun, L. Wan, X. Gu, D. Zhu, Y. Zhou, J. Chao and L. Wang, *Biosens. Bioelectron.*, 2019, **140**, 111353
14 K. Zhang, H. Dong, W. Dai, X. Meng, H. Lu, T. Wu and X. Zhang, *Anal. Chem.*, 2017, **89**, 648-655.
15 F. Yang, Y. Cheng, Y. Cao, Y. Zhang, H. Dong, H. Lu and X. Zhang, *Anal. Chem.*, **2019**, 91, 9828-9835.
16 F. Yang, Y. Cheng, Y. Cao, H. Dong, H. Lu, K. Zhang, X. Meng, C. Liu and X. Zhang, *Chem. Sci.*, 2019, **10**, 1709-1715.
17 H. Dong, J. Lei, L. Ding, Y. Wen, H. Ju and X. Zhang, *Chem. Rev.*, 2013, **113**, 6207-6233.
18 Q. Feng, X. Zhao, Y. Guo, M. Liu and P. Wang, *Biosens. Bioelectron.*, 2018, **108**, 97-102.
19 Q. Zhao, J. Piao, W. Peng, Y. Wang, B. Zhang, X. Gong and J. Chang, *ACS Appl. Mater. Interface*, 2018, **10**, 3324-3332.
20 M. Oishi and S. Sugiyama, *Small*, 2016, **12**, 5153-5158.
21 F. Zhou, Y. Yao, J. Luo, X. Zhang, Y. Zhang, D. Yin, F. Gao and P. Wang, *Anal. Chim. Acta*, 2017, **969**, 8-17.
22 J. Wang, G. Liu and M. R. Jan, *J. Am. Chem. Soc.*, 2004, **126**, 3010-3011.
23 A. Gao, N. Zou, P. Dai, N. Lu, T. Li, Y. Wang, J. Zhao and H. Mao, *Nano Lett.*, 2013, **13**, 4123-4130.
24 F. Liu, X. L. Li and H. Zhou, *Talanta*, 2020, **206**, 120199.
25 C. Zhang, P. Miao, M. Sun, M. Yan and H. Liu, *Small*, 2019, **15**, 1901867.
26 J. Zhang, S. Song, L. Zhang, L. Wang, H. Wu, D. Pan and H. C. Fan, *J. Am. Chem. Soc.*, 2006, **128**, 8575-8580.
27 X. Chen, X. Jia, J. Han, J. Ma and Z. Ma, *Biosens. Bioelectron.*, 2013, **50**, 356-361.
28 H. F. Sun, J. Chao, X. Zuo, S. Su, X. Liu, L. H. Yuwen, C. H. Fan and L. H. Wang, *RSC Adv.*, 2014, **4**, 27625-27629.
29 R. Huang, Y. Liao, X. Zhou and D. Xing, *Anal. Chim. Acta*, 2015, **888**, 162-172.
30 A. Li, J. Zhang, J. Qiu, Z. Zhao, C. Wang, C. Zhao and H. Liu, *Talanta*, 2017, **163**, 78-84.
31 W. Lai, Q. Wei, M. Xu, J. Zhuang and D. Tang, *Biosens. Bioelectron.*, 2017, **89**, 645-651.
32 L. Tang, Y. Wang, Y. Liu and J. Li, *ACS Nano*, 2011, **5**, 3817-3822.
33 W. Lu, Y. Chen, Z. Liu, W. Tang and X. Jiang, *ACS Nano*, 2016, **10**, 6685-6692.
34 Y. H. Wang, K. J. Huang, X. Wu, Y. Y. Ma, D. L. Song, C. Y. Du and S. H. Chang, *J. Mater. Chem. B*, 2018, **6**, 2134-2142.
35 L. Qiu, L. Qiu, Z. S. Wu, G. Shen and R. Q. Yu, *Anal. Chem.*, 2013, **85**, 8225-8231.
36 H. L. Shuai, K. J. Huang, W. J. Zhang, X. Cao and M. P. Jia, *Sensor. Actuat. B-Chem.*, 2017, **243**, 403-411.
37 L. Liu, N. Xia, H. Liu, X. Kang, X. Liu and C. Xue, *Biosens. Bioelectron.*, 2014, **53**, 399-405.
38 W. Nie, Q. Wang, X. Yang, H. Zhang, Z. Li, L. Gao, Y. Zheng, X. Liu and K. Wang, *Anal. Chim. Acta*, 2017, **993**, 55-62.
39 K. J. Huang, Y. J. Liu, H. B. Wang, Y. Y. Wang and Y. M. Liu, *Biosens. Bioelectron.*, 2014, **55**, 195-202.
40 L. Z. Liu, C. Song, Z. Zhang, J. Yang, L. L. Zhou, X. Zhang and G. M. Xie, *Biosens. Bioelectron.*, 2015, **70**, 351-357.

View Article Online
DOI: 10.1039/D0CC03845H

TOC

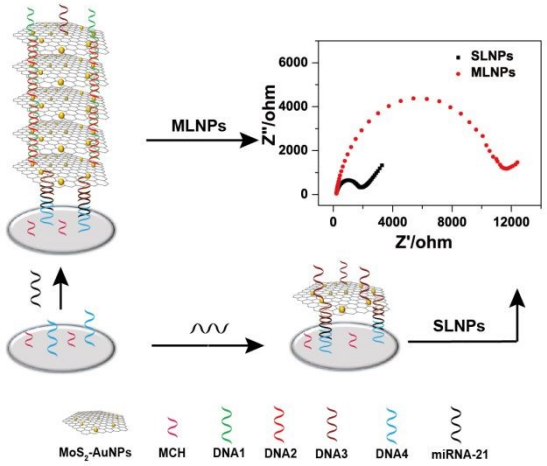

View Article Online
DOI: 10.1039/D0CC03845H

MoS_2-AuNPs-based multilayer nanoprobes is used to ultrasensitively detect microRNA-21 with ultrawide dynamic range and ultralow detection limit.